Journal of Molecular Modeling (2022) 28:324
https://doi.org/10.1007/s00894-022-05324-3

ORIGINAL PAPER

Molecular dynamics simulation of minor Zr addition on short and medium-range orders of Cu-Zr metallic glass

Xianying Cao[1] · **Minhua Sun**[2]

Received: 27 January 2022 / Accepted: 13 September 2022 / Published online: 21 September 2022

Abstract

The compositional dependence of the atomic structure and glass-forming ability (GFA) was systematically studied in a binary alloy series $Cu_{100-x}Zr_x$ ($x = 0.5$, 1.0, 2.0, 3.0, 5.0, 7.0, 10.0) by molecular dynamics simulations. Several structural analysis techniques are adopted to find a direct relationship between the atomic structures and GFA by minor Zr addition. The simulation results confirm that the difference among the critical cooling rates proves the enhancement of GFA. It is found that the Zr addition can enhance the icosahedra short-range order (SRO). From another side, in terms of MRO, the addition of Zr can enhance interpenetrating icosahedra connection which will give rise to the Bergman-icosahedra medium-range order, resulting in a more stable, more compact, and more complex structures, which is responsible for the enhanced GFA in CuZr alloys. Furthermore, the five-fold symmetry governs the formation of the amorphous state and may behave as a principal indication of the formation of the glass state during the cooling process. We also found a critical Zr content of 3%, below which the effect of Zr on the structures is not obvious. However, when the Zr content is higher than 3%, the Zr can rapidly change the structures of the liquid and glassy structure. These results are helpful for understanding the GFA of CuZr alloys.

Keyword Molecular dynamics simulation · Short-range order · Medium-range order · Metallic glasses

Introduction

In recent years, due to the broad application prospects in the industry, bulk metallic glasses (BMGs) have attracted increasing attention [1–5]. Usually, the bulk metallic glass contains multicomponent elements with a dramatic difference in the atomic size of the elements [6, 7]. Afterward, it was found that some simple binary alloy systems also show high glass-forming ability, such as Ca-Al, Cu-Zr, and Cu-Hf [8, 9]. Among these, Cu-Zr is a popular representative of early transition metallic glasses due to its high glass-forming ability (GFA) for a broad range of compositions [10–14]. It is reported that Cu-Zr binary alloys with a wide glass-forming composition range ($45 < \times < 60$ at. %) can be prepared into metallic glasses up to 2 mm in diameter by a conventional Cu-mold casting method [15–17]. Furthermore, the binary composition of Cu-Zr reduces the complexity of the possible local atomic structures, making this system ideal for the study of the evolution of the spatial structure of liquids as they are supercooled to form a glass [18–22]. Numerous studies on the GFA of the Cu-Zr binary system have been carried out both by experiments and simulation [23–26].

The high glass-forming ability of Cu-Zr alloys is usually attributed to their icosahedral orders. Strong evidence has been found that the Cu-centered full icosahedra are responsible for the high glass-forming ability of Cu-Zr BMGs [18, 27, 28]. The existence of the icosahedra (ICO) cluster increases the energy barrier to form the crystalline structures and thus improves the glass-forming ability. More importantly, the ICO clusters can be connected to each other in the cooling process to form a string like icosahedral network, the so-called medium-range order [29, 30]. There are also results related to the GFA of the Cu-Zr system to the enhanced atomic packing density by Zr addition [31, 32].

It is well known that pure Cu liquid cannot be quenched to form bulk metallic glasses. Then there raises the question as to how the Zr addition modulates the GFA and liquid structure of Cu liquids. Besides, most of the previous research focused on the compositions with the best GFA determined, such as

✉ Minhua Sun
smhua@hrbnu.edu.cn

[1] Department of Mathematics and Physics, Harbin Institute of Petroleum, Harbin 150000, China

[2] Department of Physics, Harbin Normal University, Harbin 150025, China

$Cu_{50}Zr_{50}$, $Cu_{64.5}Zr_{35.5}$, and $Cu_{64}Zr_{36}$ [33–35]. However, in such high Zr concentrations, the modulation mechanism of Zr to the liquid structure is hard to observe. It is necessary to check it from the minor Zr addition. Y. Zhang et al. studied the variation of atomic structure in $Cu_{100-x}Zr_x$ with minor Zr content ($x<10$) [36]. They found that the addition of Zr can increase the ICO short-range order. Recently, the medium-range order is also believed to be an important structural factor in determining the GFA [37]. A detailed analysis of the modulation of minor Zr to the liquid structure, especially to the medium-range structure, is crucial to understanding the GFA of CuZr alloys.

In this paper, we address these issues by conducting a systematic study using molecular dynamics (MD) simulations. We tracked the atomic structure changes, caused by minor Zr addition, especially the changes in medium-range order, to uncover the role of Zr in the improvement of GFA.

Simulation methods

Molecular dynamic simulations were carried out using the large-scale atomic/molecular massively parallel simulator (LAMMPS) [38]. Embedded atom method (EAM) potentials were used to determine interatomic interactions [39]. The time step was fixed to 2 fs in all of the simulations. Cubic simulation boxes containing 32,000 atoms were constructed by randomly distributing Cu and Zr atoms according to the stoichiometry of $Cu_{100-x}Zr_x$ with $x=0$, 0.5, 1.0, 2.0, 3.0, 5.0, 7.0, and 10.0, respectively. Periodic boundary condition was applied in all three dimensions. The simulations are performed under constant pressure and constant temperature (NPT ensemble) with zero pressure. The initial liquid state was obtained by holding the system at 1800 K for 20 ps to get a relaxed liquid state. The liquids were then quenched to 200 K with a cooling rate of 5×10^{11} K · s^{-1} to obtain glassy structures for $Cu_{100-x}Zr_x$ ($x=2.0$, 3.0, 5.0, 7.0, and 10.0). For $Cu_{100}Zr_0$, $Cu_{99.5}Zr_{0.5}$, and $Cu_{99}Zr_1$, the cooling rate is 5×10^{12} K · s^{-1}. The structural information was recorded every 100 K during the cooling process. The atomic structures were characterized using radial distribution functions (RDF) and Voronoi tessellation analysis (VTA).

The radial distribution function (RDF) which measures the probability of finding a particle at a distance r away from a given reference particle is widely used to detect the structural characteristics of glass and liquid microstructures [40, 41]. This function is defined as

$$g(r) = \frac{V}{N^2}\left\langle \sum_{i=1}^{N} \frac{n(r)}{4\pi^2\Delta r} \right\rangle \quad (1)$$

where N is the number of atoms in the simulation box, V is the volume of the box, and $n(r)$ is the number of particles located between r and r+Δr

The partial radial distribution function (PRDF) is defined as

$$g_{\alpha\beta}(r) = \frac{V}{N_\alpha N_\beta}\sum_i^N \sum_{j\neq i}^N \delta(r - r_{ij}) \quad (2)$$

where $\delta(r - r_{ij})$ is the Dirac delta function, V is the volume of the system, and N_α and N_β represent the number of α atoms and β atoms, respectively.

One of the most frequently used techniques to characterize the topological short-range order in liquid and glass structures is the VTA [42]. In this technique, the atomic arrangement around each central atom is described by four indices $<n_3,n_4,n_5,n_6>$ to differentiate between different types of the polyhedron, where n_k is the number of K-edged faces of the Voronoi polyhedron (VP). The sum of these n_k numbers represents the number of nearest-neighbor atoms, namely the coordination number (CN) for each central atom. For example, the full icosahedral motif $<0, 0, 12, 0>$ is described by twelve pentagons (n_3=0, n_4=0, n_5=12, and n_6=0).

The Bergman packing order can be confirmed by the angle distribution function (ADF) of the first and the second shell [43]. The angle is calculated according to

$$\theta_{ijk} = cos^{-1}\left(\frac{r_{ij}^2 + r_{ik}^2 - r_{jk}^2}{2r_{ij}r_{ik}}\right) \quad (3)$$

where r_{jk} is the distance between atoms j and k. j, k is the atom at the shell of the central atom i. Usually, a Bergman-type cluster is defined as one center atom-icosahedral-dodecahedral-icosahedral arrangement.

Results

The enhanced GFA by Zr addition

Figure 1 shows the radial distribution function g(r) of the $Cu_{100-x}Zr_x$ binary alloy at 200 K. The samples were obtained by quenching the liquids from 1800 K under the cooling rates of 5.0×10^{11} K · s^{-1}. From Fig. 1, the second peak exhibits pronounce split under the cooling rate of 5.0×10^{11} K · s^{-1} when the Zr atom content is greater than 3%, which indicates that the system formed typical glass structures. However, when Zr content is less than 3%, the g(r) of CuZr alloys shows sharp peaks which is the typical pattern of crystallized structure. The inset in Fig. 1 displays the g(r) of $Cu_{100}Zr_0$, $Cu_{99.5}Zr_{0.5}$, and $Cu_{99}Zr_1$ alloy under the cooling rates of 5.0×10^{12} K · s^{-1}. We found that all the alloys transformed to glassy structures when we further increased the cooling rate to 5.0×10^{12} K · s^{-1}. It shows that addition of Zr decreased the critical cooling rate and thus increased the GFA.

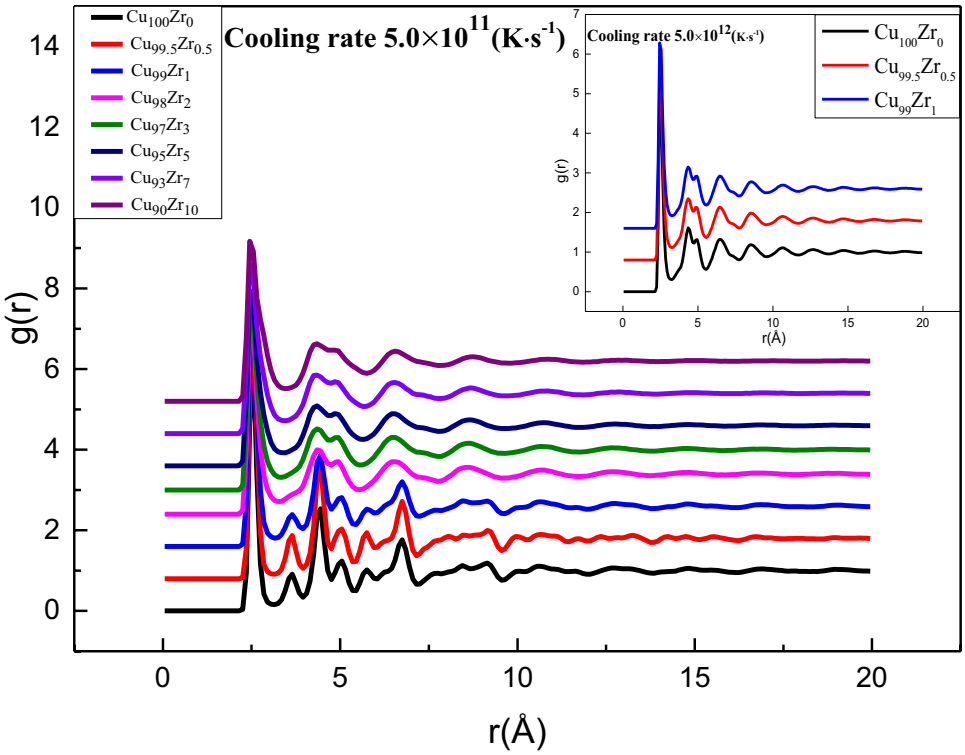

Fig. 1 Radial distribution functions g(r) of the simulated $Cu_{100-x}Zr_x$ ($x=0$, 0.5, 1.0, 2.0, 3.0, 5.0, 7.0, and 10.0) alloys at 200 K. The inset presents the g(r) of $Cu_{100}Zr_0$, $Cu_{99.5}Zr_{0.5}$, and $Cu_{99}Zr_1$ alloy under the cooling rates of 5.0×10^{12} K · s^{-1}

The temperature dependence of the atomic volume during cooling is presented in Fig. 2. At the same temperature, the atomic volume increases with increasing Zr atoms content, which is due to the larger size of Zr atoms (1.60 Å) with respect to Cu atoms (1.28 Å). The glass transition temperature, T_g, which is defined as the inflection temperature in volume-T curves can be determined and the results are also shown in Fig. 2. We can see that Tg increased monotonously from 697 to 760 K along with the Zr content increase from 0 to 10%. Although the reduced glass

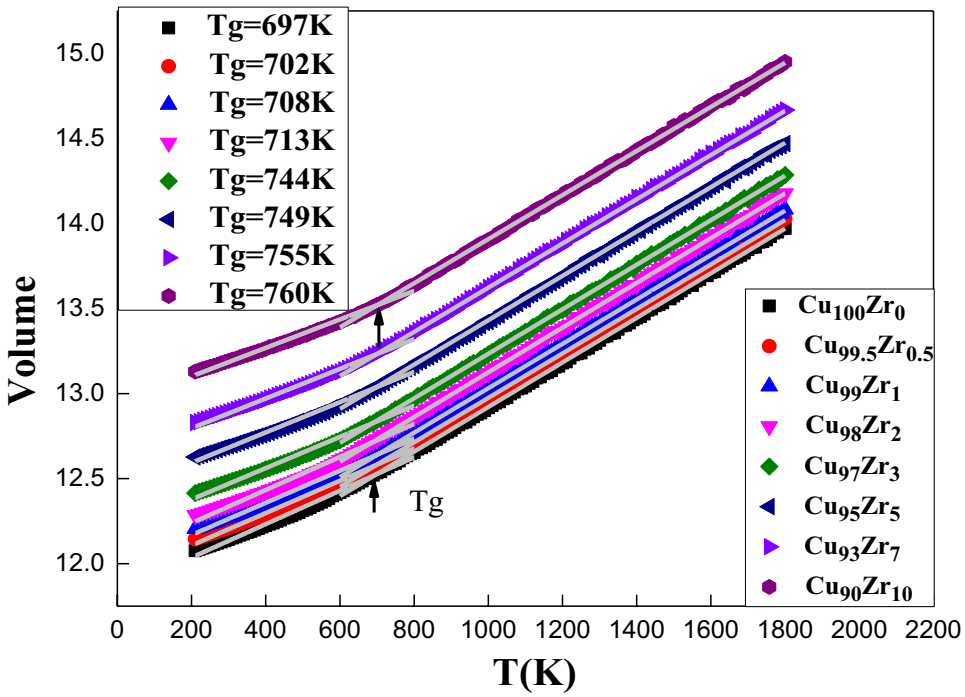

Fig. 2 Evolution of volume with temperature during cooling of $Cu_{100-x}Zr_x$ ($x=0$, 0.5, 1.0, 2.0, 3.0, 5.0, 7.0, and 10.0). The lines are linear fits in the low and high-temperature regions. The glass transition temperature T_g is determined by the intersection of the two curves

transition temperature T_{rg} is a more suitable parameter to evaluate GFA, the quick increase of T_g with minor Zr addition still provided the enhanced GFA information in CuZr alloys. For Cu-Zr system, it was found that increasing the Zr content from 0 to 10% can both decrease the critical cooling rate and increase Tg, which resulted in the increase of GFA [36].

Partial radial distribution function (PRDF)

The partial RDFs of $Cu_{100-x}Zr_x$ MGs at 200 K are shown in Fig. 3. According to Fig. 3a, little difference in the Cu-Cu partial RDFs can be observed among all the samples. Only the height of the first peak decreases as the Zr content increases. It is due to the size mismatch between the Cu and Zr atoms which will cause positions of atoms at the nearest neighbor to become more dispersed. It also can be found that a slight bump at 3.6 Å disappears with the increase of Zr which shows the transformation of the liquid structure from a crystalline characteristic to a homogeneous liquid structure. For Cu-Zr partial RDFs which is shown in Fig. 3b, an increase in the amplitudes of the first maxima shows that Cu atoms prefer to bond with Zr atoms. Besides these, we cannot get further structure information caused by Zr addition from the partial RDFs.

Voronoi tessellation analysis

We employ the Voronoi tessellation analysis method to characterize the local atomic structure of configurations. In Fig. 4, we show the fractions of the top ten of the most dominant Voronoi polyhedron (VP) in CuZr metallic glass at 200 K. In general, the types of VP can be divided into three categories. The "crystal-like" represents a quasi-crystalline structure and is indexed by Voronoi polyhedral type $<0, 4, 4, x>$ with $x=5, 6, 7$. The "Mixed" type is a category that consisted of $<0, 3, 6, x>$ with $x=4, 5$, and 6. The "ICO-like" type, such as $<0, 1, 10, 2>$, $<0, 0, 12, 0>$, $<0, 2, 8, 2>$, $<0, 1, 10, 3>$ and $<0, 2, 8, 4>$, are the VPs with high n_5 value (n_5=8, 10, or 12) which characterizes perfect and defective icosahedral structures [44]. From Fig. 4, we found that the fraction of "ICO-like" VPs increases significantly with the Zr addition. While the fraction of "mixed" VPs, which is $<0, 3, 6, 4>$, $<0, 3, 6, 5>$, and $<0, 3, 6, 6>$ and the "crystal-like" VPs, which is $<0, 4, 4, 6>$ and $<0, 4, 4, 7>$ decrease with increasing Zr atom content. These results indicate the ability of Zr atoms to promote the formation of ICO clusters and strongly increase the icosahedral short-range order in the system.

The evolution of the three types of VPs as a function of the temperature during the cooling process is presented in Fig. 5. Figure 5a shows the increased fraction of "crystal-like" VPs with decreasing temperature. We can divide the curves into two groups according to their variation behavior below T_g. When the Zr content is higher than 3%, the "crystal-like" VPs increase slowly with temperatures; while the Zr content is lower than 3%, the "crystal-like" VPs increase much faster. It confirms that crystallization is impeded by the higher content of Zr addition. These two categories can also be clearly observed in Fig. 5b and c, in which the variation of the "Mixed" VPs and "ICO-like" VPs is plotted. It shows that there exists a critical Zr content which is 3%. When the Zr content is lower than 3%, the Zr addition only slightly modifies the liquid structure of copper. However, when the Zr addition is higher

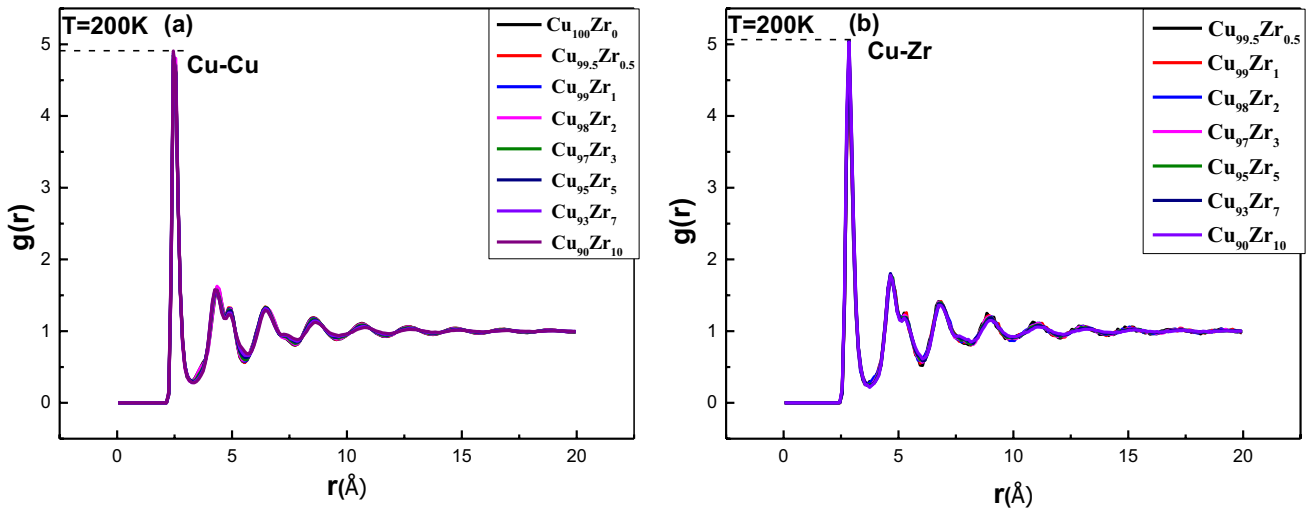

Fig. 3 The partial RDFs of the simulated $Cu_{100-x}Zr_x$ systems at 200 K. **a** Cu-Cu partial RDFs; **b** Cu-Zr partial RDFs

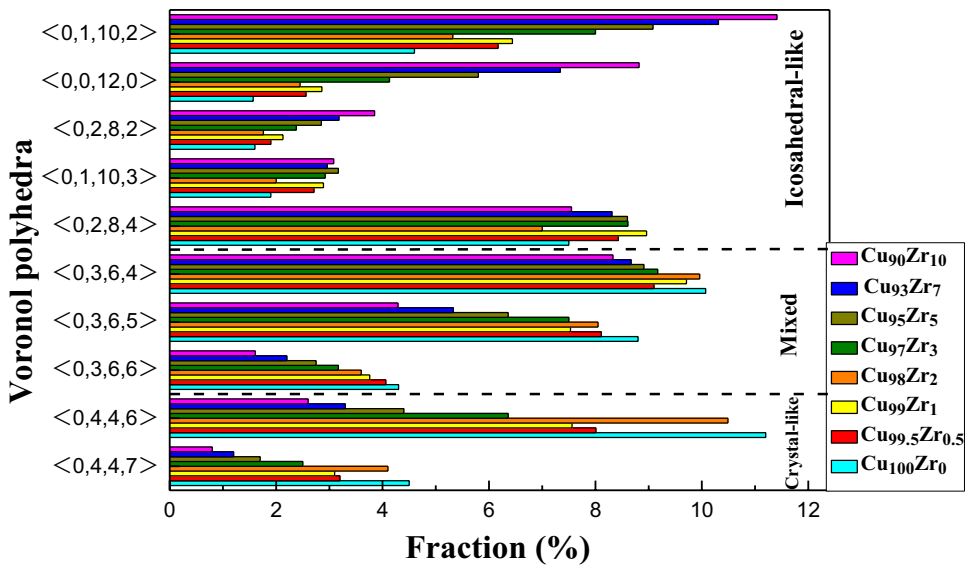

Fig. 4 Distribution of the top ten most dominant Voronoi polyhedral at 200 K for $Cu_{100-x}Zr_x$ ($x = 0$, 0.5, 1.0, 2.0, 3.0, 5.0, 7.0, and 10.0)

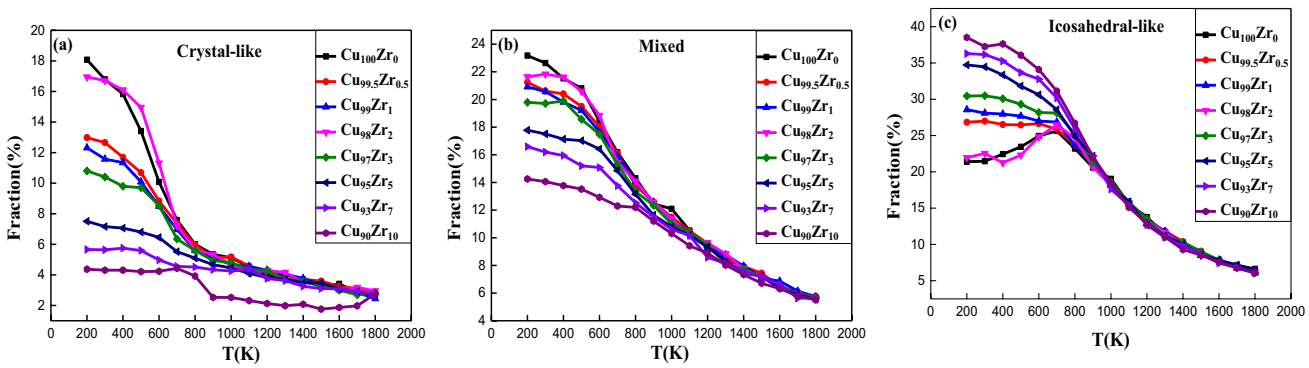

Fig. 5 **a** The fraction of "crystal-like" clusters with decreasing temperature for $Cu_{100-x}Zr_x$. **b** The fraction of "mixed-like" clusters. **c** The fraction of "ICO-like" clusters

than 3%, the liquid turns rapidly to ICO-dominated glass-forming liquids. It indicates that there exist two distinct glass states before and after 3% Zr contents.

The two distinct glassy states can also be confirmed from the angle distribution function (ADFs), which are shown in Fig. 6. When the Zr content is lower than 3%, there are four characteristic angles in the ADFs, which are 43°, 58°, 92°, and 117°, respectively. These angles demonstrate that there are plenty of crystalline-like clusters of the liquids. When the Zr content is higher than 3%, the angle of 43° disappears and the angles of 92° and 117° merged into a new angle of 112°. We should note that the two peaks in higher Zr content are consistent with the characteristic peak of ICO short-range order, which is 58° and 112° [45]. This suggests that the glass-forming liquid with strong ICO short-range order can only be obtained when the Zr addition is higher than the critical content of 3%.

Medium-range order

Next, we checked how the Zr addition affects the medium-range order of the icosahedral cluster in CuZr binary alloy. First, we analyzed the network formed by < 0, 0, 12, 0 > VPs. The number of ICO clusters in the cooling process in $Cu_{100-x}Zr_x$ alloy is calculated and shown in Fig. 7. In Fig. 7, two distinct ICO-connected paths can also be observed. The number of ICO clusters is almost maintained constant when Zr content is less than 3%. However, in the case of Zr content higher than 3%, the number of icosahedral clusters first increases rapidly with decreasing temperatures and then decreases rapidly as the temperature decreases from 1000 K. It shows the pic of the increasement and connection of ICO VPs in the cooling process. Zr contents contribute to the formation of ICO clusters and then help the ICO clusters to aggregate into a

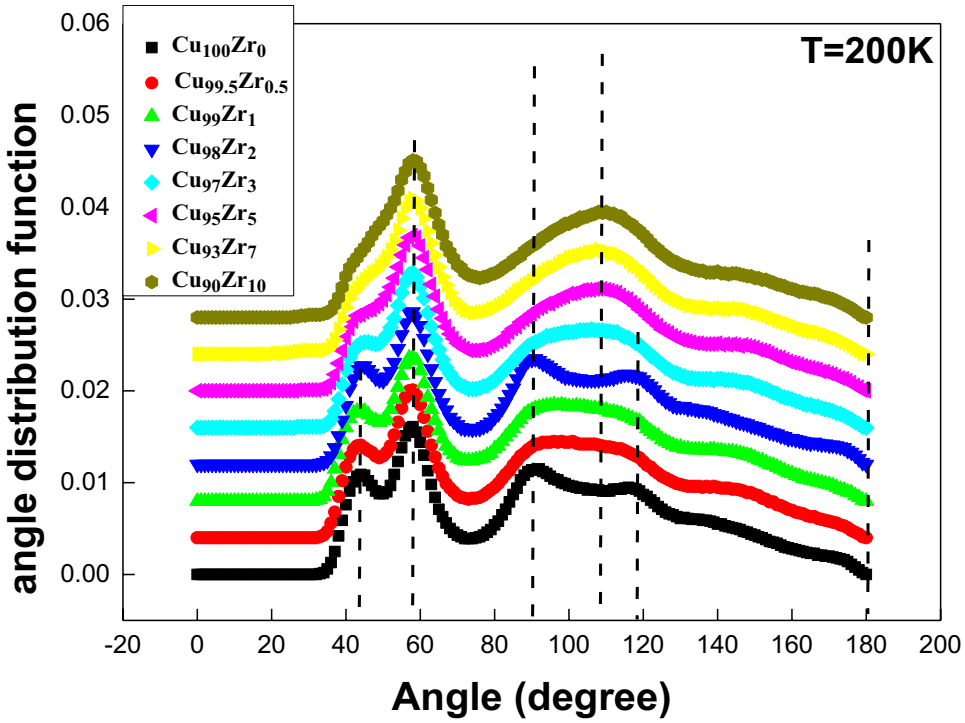

Fig. 6 ADFs of the first shell of $Cu_{100-x}Zr_x$ MGS at 200 K. The characteristic angle of ICO is also plotted in dashed lines

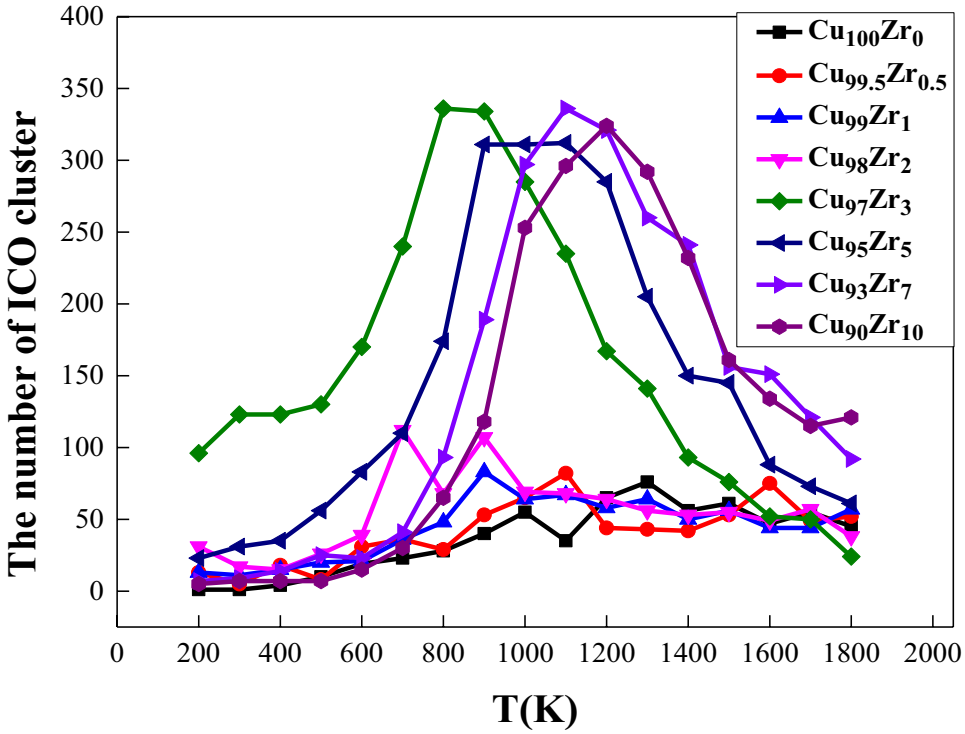

Fig. 7 The amounts of icosahedra cluster with temperature in $Cu_{100-x}Zr_x$ ($x = 0$, 0.5, 1.0, 2.0, 3.0, 5.0, 7.0, and 10.0)

larger network, which will create ICO medium-range order (MRO) in the liquids.

There are four different linkages between two icosahedra, which is intercross-sharing (IS), face-sharing (FS), edge-sharing (ES), and vertex-sharing (VS) cluster respectively. The variation of the four linkages numbers in the system at 200 K is shown in Fig. 8. The connected ICO populations are close to zero when Zr atomic content is less than 3%, while the connections of ICO increase rapidly when Zr atomic content is greater than 3%. Among the four linkages,

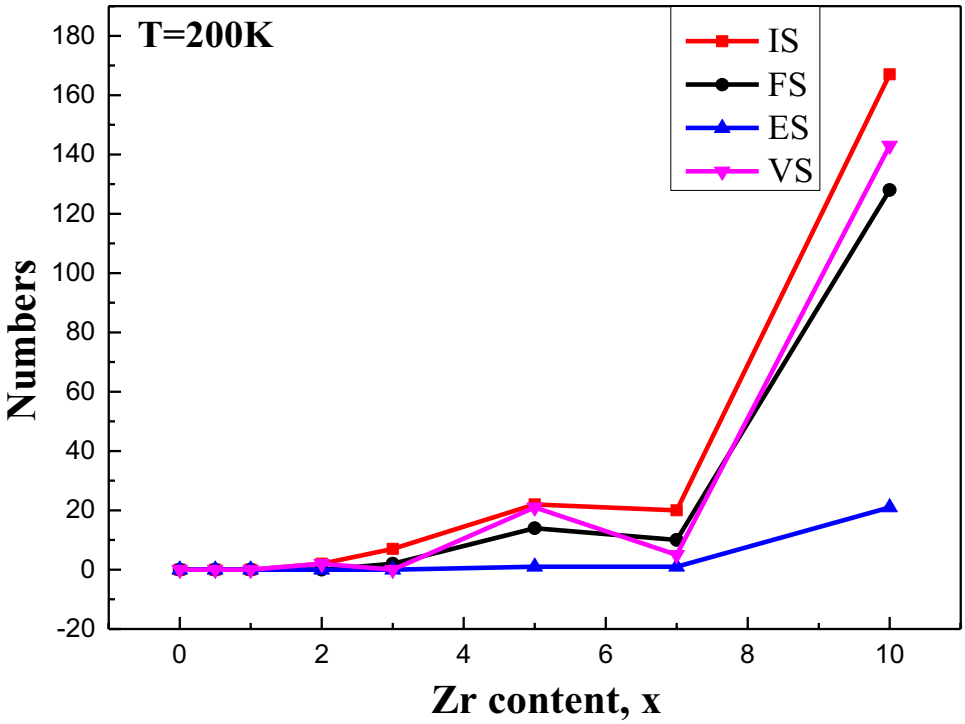

Fig. 8 Population of IS, FS, ES, and VS linkages with Zr content at 200 K

the IS linkage mode is the dominant one. The ICO clusters connected by IS can exhibit a more locally ordered structure and show a higher atomic packing density than other linkages and make the structure more stable to resist crystallization [46].

We also calculated the sharing coordination atoms (SCA) between the central atom and one of its second shell atoms. It is an indicator parameter of MRO and can be used to describe packing feathers in the second neighbor shells. The details of SCA methods can be found in ref [47]. In ICO-type metallic glass, the SCA-3 is the characteristic index of Bergman MRO while the SCA-2 is more related to the Mackay MRO [48]. Figure 9 shows the variation of the SCA index with increasing Zr atom content at 200 K. We found that the SCA-1 index is almost kept constant with Zr addition. However, the SCA-2 and SCA-4 index

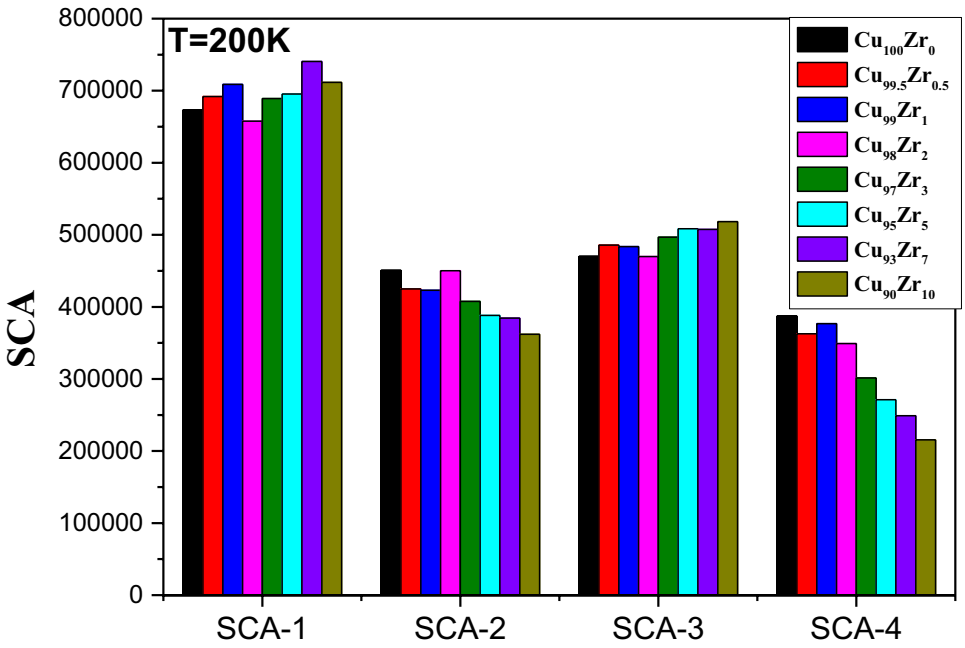

Fig. 9 Variation of the four main SCA indexes with increasing Zr content at 200 K

decrease with increasing Zr content, while the SCA-3 index increases. Meanwhile, the SCA-3 index is higher than the SCA-2 index, which demonstrates that the addition of Zr enhances the Bergman MRO in the system [47]. Since the SCA-4 corresponds to a much looser packing method, the decreasing of SCA-4 methods shows the atomic packing become denser with the Zr addition.

To analyze the detailed MRO change in the system by Zr addition, we picked all the ICO-centered atoms and calculated their RDFs which are shown in Fig. 10. The RDFs show sharp first peaks which correspond to the IS connection of ICO VPs. And the RDFs also show clearly four or five following peaks beyond the first sharp peaks which show MRO structures formed in the liquid. We normalized all the peak positions in RDFs with the position of the first peak, and we get the normalized peak positions. The results are shown in Table 1. We found that the normalized peaks show a sequence of 1, 1.66, 2.01, 2.5, 2.6, and 3.04 in $Cu_{100-x}Zr_x$ binary alloy. This sequence corresponds well to the six shells of the Bergman structure, which are 1.0, 1.58, 2.00, 2.42, 2.67, and 3.00 [47]. These results confirm that enhanced Bergman-ICO type of MRO with the Zr additions.

Discussion

As illustrated above, the addition of Zr content can decrease the critical cooling rate and increase T_g. From Voronoi analysis results, we find that the Zr addition leads to the enhancement of ICO short-range order. More importantly,

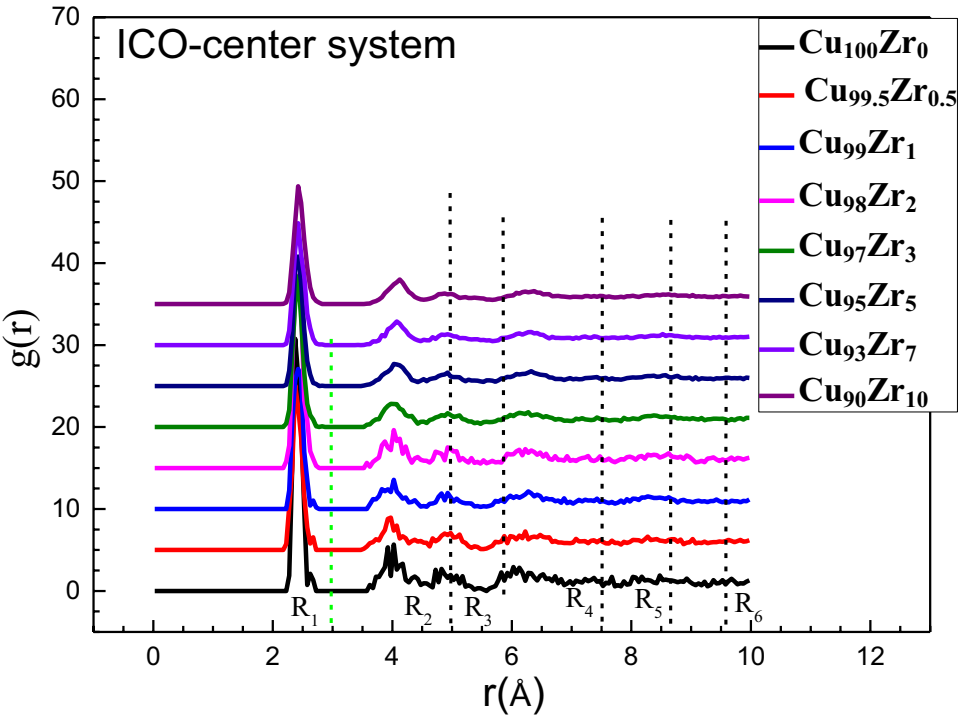

Fig. 10 The RDFs of the ICO-center system for the $Cu_{100-x}Zr_x$ ($x = 0$, 0.5, 1.0, 2.0, 3.0, 5.0, 7.0, and 10.0)

Table 1 Comparison of the RDF peaks with hierarchical ICO structure of the $Cu_{100-x}Zr_x$. All the peak positions are normalized by the position of the first peak of RDF

	R_1/R_1	R_2/R_1	R_3/R_1	R_4/R_1	R_5/R_1	R_6/R_1
$Cu_{100}Zr_0$	1	1.66	1.99	2.48	2.59	3.04
$Cu_{99.5}Zr_{0.5}$	1	1.68	2.01	2.5	2.6	3.04
$Cu_{99}Zr_1$	1	1.66	1.99	2.5	2.59	3.04
$Cu_{98}Zr_2$	1	1.66	2.01	2.5	2.6	3.04
$Cu_{97}Zr_3$	1	1.66	1.99	2.5	2.6	3.04
$Cu_{95}Zr_5$	1	1.66	1.99	2.5	2.6	3.04
$Cu_{93}Zr_7$	1	1.68	1.99	2.5	2.6	3.04
$Cu_{90}Zr_{10}$	1	1.68	2.01	2.5	2.6	3.04
Hierarchical ICO structure	1	1.58	2.00	2.42	2.67	3.00

the addition of Zr can enhance interpenetrating ICO connection which will give rise to the Bergman-ICO medium order in the glasses. As a result, the addition of Zr makes the Cu-Zr binary alloy not only energetically more favorable but also structurally more stable [49]. The ICO order with a fivefold environment can increase the barrier for nucleation and cause slower structural rearrangement [50, 51] and therefore retard the nucleation of crystals, leading to the enhancement of GFA [52, 53]. This is the structural origin of Zr to improve the GFA of CuZr alloys. Our results also found that there exists a critical Zr content which is 3%. The glass states show distinct structural characters before and after 3%.

Conclusions

In summary, molecular dynamics simulation is performed to investigate the structural behavior of CuZr binary alloy by minor Zr addition. Various techniques have been used to characterize the atomic-level structure in terms of short-to-medium range order. Our results demonstrate that the slight change in the composition of Zr can significantly influence the microstructure of CuZr metallic glass. We found that the GFA can be greatly enhanced by minor Zr additions. The Zr addition can enhance the ICO short-range order (SRO) of the system, and the main connection method of ICO clusters is IS linkage. In the medium range, Bergman MRO becomes stronger with Zr addition. The improvement of SRO and MRO is responsible for the enhanced GFA in CuZr alloys, and we also found a critical Zr content which is 3%. When the Zr content is lower than 3%, the effect of Zr on the structures is not obvious. However, when the Zr content is higher than 3%, the Zr can rapidly change the structures of the liquid and glassy structure. Our results help to elucidate the role of Zr in CuZr metallic glasses from the atomic level.

Author contribution All the authors contributed to the conceptualization, formal analyses, investigation, writing—original draft, and writing—review and editing the manuscript. Xianying Cao was also responsible for funding acquisition, resources, and supervision.

Funding This research was supported by the Natural Science Foundation Joint guidance project of Heilongjiang Province from China (Grant No. LH2020E095).

Data availability The datasets generated during and/or analyzed during the current study are available from the corresponding author on reasonable request.

Declarations

Conflict of interest The authors declare no competing interests.

References

1. Greer AL (1993) Confusion by design. Nature 366:303–304
2. Inoue A (2000) Stabilization of metallic supercooled liquid and bulk amorphous alloys. Acta Mater 48:279–306. https://doi.org/10.1016/S1359-6454(99)00300-6
3. Louzguine-Luzgin DV, Inoue A (2013) Bulk metallic glasses: formation, structure, properties, and applications, in: Handbook of magnetic materials, Elsevier, pp. 131–171.
4. Khan MM, Nemati A, Rahman ZU, Shah UH, Asgar H, Haider W (2018) Recent advancements in bulk metallic glasses and their applications: a review. Crit Rev Solid State Mater Sci 43:233–268
5. Qin C, Zhao W, Inoue A (2011) Glass formation, chemical properties and surface analysis of Cu-based bulk metallic glasses. Int J Mol Sci 12:2275–2293
6. Cheng Y, Ma E, Sheng H (2009) Atomic level structure in multicomponent bulk metallic glass. Phys Rev Lett 102:245501
7. Takeuchi A, Chen N, Wada T, Yokoyama Y, Kato H, Inoue A, Yeh J (2011) Pd20Pt20Cu20Ni20P20 high-entropy alloy as a bulk metallic glass in the centimeter. Intermetallics 19:1546–1554
8. Duan G, Xu D, Zhang Q, Zhang G, Cagin T, Johnson WL, Goddard WA III (2005) Molecular dynamics study of the binary Cu 46 Zr 54 metallic glass motivated by experiments: Glass formation and atomic-level structure. Phys Rev B 71:224208
9. Zhu Z, Zhang H, Pan D, Sun W, Hu Z (2006) Fabrication of Binary Ni-Nb bulk metallic glass with high strength and compressive plasticity. Adv Eng Mater 8:953–957
10. Sha Z, Xu B, Shen L, Zhang A, Feng Y, Li Y (2010) The basic polyhedral clusters, the optimum glass formers, and the composition-structure-property (glass-forming ability) correlation in Cu–Zr metallic glasses. J Appl Phys 107:063508
11. Chang TY, Wang Z, Xu D (2021) Icosahedral clusters in Cu100-xZrx (x= 32, 34, 36, 38.2, 40 at%) metallic glasses near the peak of glass-forming ability (x= 36): a balance between population and encaging strength. J Phys Chem Solids 154:110076
12. Kwon O, Kim Y, Kim K, Lee Y, Fleury E (2006) Formation of amorphous phase in the binary Cu− Zr alloy system. Met Mater Int 12:207–212
13. Bendert J, Gangopadhyay A, Mauro N, Kelton K (2012) Volume expansion measurements in metallic liquids and their relation to fragility and glass forming ability: an energy landscape interpretation. Phys Rev Lett 109:185901
14. Apreutesei M, Steyer P, Billard A, Joly-Pottuz L, Esnouf C (2015) Zr–Cu thin film metallic glasses: An assessment of the thermal stability and phases' transformation mechanisms. J Alloy Compd 619:284–292
15. Xu D, Lohwongwatana B, Duan G, Johnson WL, Garland C (2004) Bulk metallic glass formation in binary Cu-rich alloy series–Cu100− xZrx (x= 34, 36, 38.2, 40 at.%) and mechanical properties of bulk Cu64Zr36 glass. Acta Materialia 52:2621–2624
16. Löffler JF (2003) Bulk metallic glasses. Intermetallics 11:529–540
17. Zhang A, Chen D, Chen Z (2009) Bulk metallic glass-forming region of Cu–Zr binary and Cu–Zr based multicomponent alloy systems. J Alloy Compd 477:432–435
18. Lee M, Lee C-M, Lee K-R, Ma E, Lee J-C (2011) Networked interpenetrating connections of icosahedra: effects on shear transformations in metallic glass. Acta Mater 59:159–170
19. Schenk T, Holland-Moritz D, Simonet V, Bellissent R, Herlach D (2002) Icosahedral short-range order in deeply undercooled metallic melts. Phys Rev Lett 89:075507
20. Cheng Y, Cao A, Ma E (2009) Correlation between the elastic modulus and the intrinsic plastic behavior of metallic glasses: the roles of atomic configuration and alloy composition. Acta Mater 57:3253–3267

21. Nelson DR (1983) Order, frustration, and defects in liquids and glasses. Phys Rev B 28:5515
22. Wakeda M, Shibutani Y (2010) Icosahedral clustering with medium-range order and local elastic properties of amorphous metals. Acta Mater 58:3963–3969
23. Baser T, Das J, Eckert J, Baricco M (2009) Glass formation and mechanical properties of (Cu50Zr50) 100− xAlx (x= 0, 4, 5, 7) bulk metallic glasses. J Alloy Compd 483:146–149
24. Cheng Y, Ma E, Sheng H (2008) Alloying strongly influences the structure, dynamics, and glass forming ability of metallic supercooled liquids. Appl Phys Lett 93:111913
25. Hao S, Wang C, Kramer M, Ho K (2010) Microscopic origin of slow dynamics at the good glass forming composition range in Zr 1− x Cu x metallic liquids. J Appl Phys 107:053511
26. Lu B, Kong L, Laws K, Xu W, Jiang Z, Huang Y, Ferry M, Li J, Zhou Y (2018) EXAFS and molecular dynamics simulation studies of Cu-Zr metallic glass: short-to-medium range order and glass forming ability. Mater Charact 141:41–48
27. Ritort F, Sollich P (2003) Glassy dynamics of kinetically constrained models. Adv Phys 52:219–342
28. Cheng Y, Sheng H, Ma E (2008) Relationship between structure, dynamics, and mechanical properties in metallic glass-forming alloys. Phys Rev B 78:014207
29. Wu Z, Li M, Wang W, Liu K (2013) Correlation between structural relaxation and connectivity of icosahedral clusters in CuZr metallic glass-forming liquids. Phys Rev B 88:054202
30. Foroughi A, Tavakoli R, Aashuri H (2016) Molecular dynamics study of structural formation in Cu50–Zr50 bulk metallic glass. J Non-Cryst Solids 432:334–341
31. Lu B, Kong L, Jiang Z, Huang Y, Li J, Zhou Y (2014) Roles of alloying additions on local structure and glass-forming ability of Cu–Zr metallic glasses. J Mater Sci 49:496–503
32. Aliaga LCR, Lima LV, Domingues GM, Bastos IN, Evangelakis GA (2019) Experimental and molecular dynamics simulation study on the glass formation of Cu–Zr–Al alloys. Materials Research Express 6:045202
33. Peng H, Li M, Wang W, Wang C-Z, Ho K (2010) Effect of local structures and atomic packing on glass forming ability in Cu x Zr 100–x metallic glasses. Appl Phys Lett 96:021901
34. Tian H, Zhang C, Wang L, Zhao J, Dong C, Wen B, Wang Q (2011) Ab initio molecular dynamics simulation of binary Cu64Zr36 bulk metallic glass: validation of the cluster-plus-glue-atom model. J Appl Phys 109:123520
35. Ghaemi M, Tavakoli R, Foroughi A (2018) Comparing short–range and medium–range ordering in CuZr and NiZr metallic glasses–correlation between structure and glass form ability. J Non-Cryst Solids 499:227–236
36. Zhang Y, Mattern N, Eckert J (2012) Study of direct relationship between atomic structures and glass forming abilities of Cu100-x Zrx (0≤ x≤ 10) liquids by molecular dynamics simulations. J Appl Phys 111:053520
37. Wu N, Yan M, Zuo L, Wang J (2014) Correlation between medium-range order structure and glass-forming ability for Al-based metallic glasses. J Appl Phys 115:043523
38. Sheng H, Kramer M, Cadien A, Fujita T, Chen M (2011) Highly optimized embedded-atom-method potentials for fourteen fcc metals. Phys Rev B 83:134118
39. Daw MS, Baskes MI (1983) Semiempirical, quantum mechanical calculation of hydrogen embrittlement in metals. Phys Rev Lett 50:1285
40. Daw MS, Baskes MI (1984) Embedded-atom method: derivation and application to impurities, surfaces, and other defects in metals. Phys Rev B 29:6443
41. Nguyen TD, Nguyen CC, Tran VH (2017) Molecular dynamics study of microscopic structures, phase transitions and dynamic crystallization in Ni nanoparticles. RSC Adv 7:25406–25413. https://doi.org/10.1039/C6RA27841H
42. Trady S, Hasnaoui A, Mazroui M (2017) Atomic packing and medium-range order in Ni3Al metallic glass. J Non-Cryst Solids 468:27–33
43. Sheng H, Luo W, Alamgir F, Bai J, Ma E (2006) Atomic packing and short-to-medium-range order in metallic glasses. Nature 439:419–425
44. Guo Y, Qiao C, Wang J, Shen H, Wang S, Zheng Y, Zhang R, Chen L, Su W-S, Wang C-Z (2019) Bergman-type medium range order in amorphous Zr77Rh23 alloy studied by ab initio molecular dynamics simulations. J Alloy Compd 790:675–682
45. Cheng Y, Ma E (2011) Atomic-level structure and structure–property relationship in metallic glasses. Prog Mater Sci 56:379–473
46. Kuo K (2002) Mackay, anti-Mackay, double-Mackay, pseudo-Mackay, and related icosahedral shell clusters. Struct Chem 13:221–230
47. Sun M, Han C, Lan Y (2021) Hierarchical fivefold symmetry in CuZr metallic glasses. J Non-Cryst Solids 555:120548
48. Fang X, Wang C-Z, Hao S, Kramer MJ, Yao Y, Mendelev M, Ding Z, Napolitano R, Ho K-M (2011) Spatially resolved distribution function and the medium-range order in metallic liquid and glass. Sci Rep 1:1–5
49. Xie Z-C, Gao T-H, Guo X-T, Qin X-M, Xie Q (2014) Glass formation and icosahedral medium-range order in liquid Ti–Al alloys. Comput Mater Sci 95:502–508
50. Dzugutov M, Simdyankin SI, Zetterling FH (2002) Decoupling of diffusion from structural relaxation and spatial heterogeneity in a supercooled simple liquid. Phys Rev Lett 89:195701
51. Zetterling F, Dzugutov M, Simdyankin S (2001) Formation of large-scale icosahedral clusters in a simple liquid approaching the glass transition. J Non-Cryst Solids 293:39–44
52. Xi XK, Li LL, Zhang B, Wang WH, Wu Y (2007) Correlation of atomic cluster symmetry and glass-forming ability of metallic glass. Phys Rev Lett 99:095501
53. Wang Q, Liu CT, Yang Y, Dong Y, Lu J (2011) Atomic-scale structural evolution and stability of supercooled liquid of a Zr-based bulk metallic glass. Phys Rev Lett 106:215505